Int. J. Heat Mass Transfer. Vol. 32, No. 1, pp. 171–181, 1989
Printed in Great Britain

0017–9310/89 $3.00 + 0.00

Experimental and numerical study of natural convection between two eccentric tubes

D. NAYLOR
Faculty of Engineering Science, University of Western Ontario,
London, Ontario, Canada N6A 5B9

H. M. BADR
Mechanical Engineering Department, King Fahd University of Petroleum & Minerals,
KFUMP Box 322, Dhahran 31261, Saudi Arabia

and

J. D. TARASUK
Department of Mechanical Engineering, Faculty of Engineering Science,
University of Western Ontario, London, Ontario, Canada N6A 5B9

(*Received* 14 *January* 1988 *and in final form* 14 *June* 1988)

Abstract—An experimental and numerical study is performed on natural convection heat transfer from a horizontal isothermal inner tube to a surrounding isothermal outer tube. Experimental results are obtained using a Mach–Zehnder interferometer and the governing equations are solved numerically using a variational finite element method. Emphasis is given to the effect of inner tube eccentricity and azimuthal angular location on the thermal field in the annulus. Results are obtained for air at three specific Rayleigh numbers in the transition regime, $Ra = 5 \times 10^2$, 10^3, 1.5×10^3.

INTRODUCTION

NATURAL convection in the horizontal concentric annulus has been extensively studied due to its broad industrial applications. This geometry is used to insulate parabolic solar collectors and underground pipelines. Also, underground high voltage cables are cooled and electrically insulated with an annular gap of gas.

Natural convection in an eccentric annulus has been studied to a lesser extent. Eccentricity alters the size and the strength of the convective cells in the annulus and produces a decreased resistance to conductive heat transfer. By judicious design for a given application, the effect of eccentricity could be utilized to improve the thermal characteristics of the fluid-filled gap.

The bulk of previous experimental studies of the eccentric geometry are primarily concerned with the variation of overall heat transfer with eccentricity and Rayleigh number. Such studies are those by Koshmarov and Ivanov [1], Probert *et al.* [2] and Sande and Hamer [3]. However, detailed interferometric results for both vertical and non-vertical eccentricities have been presented by Kuehn and Goldstein [4] in the boundary layer regime ($3 \times 10^4 < Ra < 10^5$). In the boundary layer regime the overall heat transfer coefficients were all within 10% of the concentric geometry for $e/L = 1/3, 2/3$.

Extensive numerical studies for the eccentric geometry have been performed over a wide range of eccentricity and Rayleigh numbers. References [5, 6] studied vertical eccentricities, while Cho *et al.* [7] and Projahn *et al.* [8], extended these results to non-vertical eccentricities. Where feasible, the numerical predictions were verified by comparison with the interferometric results of Kuehn and Goldstein [4] in the boundary layer regime ($Ra = 4.9 \times 10^4$).

The primary objective of this study is to extend the knowledge of the temperature distributions, local heat transfer distributions and overall heat transfer for vertical and non-vertical eccentricities at low Rayleigh number. As shown in Fig. 1, the present study investigates the influence of eccentricity (e), azimuthal angle (η), and Rayleigh number on the convective heat transfer through air between the horizontal isothermal cylinders.

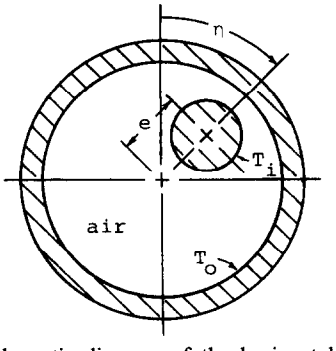

FIG. 1. A schematic diagram of the horizontal eccentric annulus.

NOMENCLATURE

C_p	constant pressure specific heat
D_i	inner tube diameter
D_o	outer tube diameter
e	eccentricity
g	gravitational acceleration
k	thermal conductivity
K_{eq}	local equivalent conductivity
$\bar{K}_{eq}$	average equivalent conductivity
L	average gap width, $(D_o - D_i)/2$
Pr	Prandtl number
q	rate of heat transfer per unit area
r	radius
R_i	inner tube radius
R_o	outer tube radius
Ra	Rayleigh number, $\rho g \beta L^3 (T_i - T_o)/\mu\alpha$
T	temperature
T_i	inner tube temperature
T_o	outer tube temperature
u, v	dimensionless velocity components in the x- and y-directions
u', v'	velocity components in the x'- and y'-directions
x, y	dimensionless Cartesian coordinates
x', y'	Cartesian coordinates.

Greek symbols

α	thermal diffusivity
β	volumetric thermal expansion coefficient
ξ	dimensionless vorticity
ξ'	vorticity
η	azimuthal angle
θ_i	angular location on the inner tube
θ_o	angular location on the outer tube
μ	dynamic viscosity
ρ	fluid density
Φ	dimensionless temperature
ψ	dimensionless stream function
ψ'	stream function.

Subscripts

cond	conduction
conv	convection
i	inner tube
o	outer tube.

EXPERIMENTAL APPARATUS AND PROCEDURE

To obtain comprehensive data for comparison with the numerical solution, a test section 40 cm long was constructed for use in a Mach–Zehnder interferometer. A sketch of the test section is shown in Fig. 2.

The outer aluminum tube (25.10 mm i.d.) of the test section was cooled by water supplied from a constant head tank. The cooling water flowed through a copper tube wound helically onto its outer surface. A nichrome wire heated the copper inner tube (9.66 mm o.d.) along its center line. Two stainless steel rods (2 mm diameter) supported the inner tube. The eccentricity could be set by turning the nut adjustments on the top of the test section. The entire test section was rotated to obtain the desired azimuthal angle.

The surface temperatures in the test section were measured using copper–constantan thermocouples. Twelve thermocouples recorded the axial and circumferential temperature gradients on the outer tube. The outer tube was isothermal in the circumferential direction within 0.1°C and axially isothermal within 0.2°C. Due to space limitations, only two thermocouples were used to measure the inner tube's surface temperature. Taking advantage of axial symmetry, one thermocouple was located at the midsection of the inner tube and the other 16 mm from one end. With 20 mm of extra heating wire coiled near each end to compensate for end heat losses, the maximum temperature difference in the inner tube for any experiment was 0.6°C at an overall temperature difference of $T_i - T_o = 46$°C.

A total of 33 interferograms were taken involving eleven eccentric positions of the inner tube at three Rayleigh numbers. Air was the test fluid for all experiments. The range of variables is summarized below:

$$D_o/D_i = 2.6$$
$$e/L = 0, 0.3, 0.6$$
$$\eta = 0°, 45°, 90°, 135°, 180°$$
$$Ra = 5.0 \times 10^2, 1.0 \times 10^3, 1.5 \times 10^3.$$

The lower and upper limits of Rayleigh number were set by lack of fringes and refraction effects, respectively. For each experiment, the power input to the inner tube was manually adjusted to yield the desired steady-state Rayleigh number within 1%.

Local heat transfer results were obtained by viewing the interferogram negatives with a travelling microscope. Local equivalent conductivities were calculated at 15° increments from scans of the closest two destructive fringes perpendicular to the inner and outer tube surfaces. Since the fluid velocity is low near the surface, the temperature field is conduction dominated and logarithmic extrapolation reflects the nature of conduction in the cylindrical layer. Hence, the surface temperature gradients were calculated using the first two optically determined fringe temperatures (T_1, T_2) and fringe radii (r_1, r_2) as

$$\left.\frac{dT}{dr}\right|_{r=R_i} = \frac{(T_1 - T_2)}{R_i \ln (r_1/r_2)} \tag{1}$$

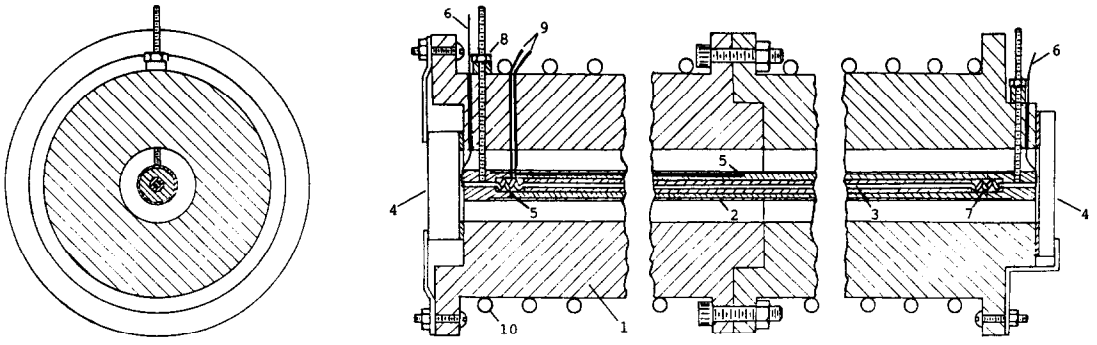

FIG. 2. Cross-sectional diagram of the test section: 1, outer tube; 2, inner tube; 3, nichrome heating wire; 4, optical windows; 5, thermocouple locations in the inner tube; 6, electrical connections; 7, extra heating wire; 8, eccentricity adjustment; 9, inner tube thermocouples; 10, copper cooling water tube.

for the inner tube, and

$$\left.\frac{dT}{dr}\right|_{r=R_o} = \frac{(T_1 - T_2)}{R_o \ln(r_1/r_2)} \tag{2}$$

for the outer tube.

The local equivalent conductivity was calculated as

$$K_{eq} = \frac{q_{conv}}{q_{cond}} \tag{3}$$

where q is the local rate of heat transfer per unit area and subscripts cond and conv refer to the conduction and convection modes of heat transfer. It is important to note that q_{cond} is for the case of the concentric geometry.

Simpson's rule (with no end corrections) was used to integrate the outer tube's local equivalent conductivity distribution to obtain the average equivalent conductivity, $\bar{K}_{eq}$. Details of the experimental apparatus, test section and data reduction are given in ref. [9].

NUMERICAL PROCEDURE

The buoyancy driven flow in the annulus between the two tubes is assumed to be laminar based on the results of Kuehn and Goldstein [4]. Using the Boussinesq approximation, the conservation equations of mass, momentum and energy for steady two-dimensional incompressible flow of a viscous fluid can be expressed as

$$u\frac{\partial \xi}{\partial x} + v\frac{\partial \xi}{\partial y} = Pr\nabla^2\xi + Ra\,Pr\frac{\partial \Phi}{\partial x} \tag{4}$$

$$-\xi = \nabla^2\psi \tag{5}$$

$$u\frac{\partial \Phi}{\partial x} + v\frac{\partial \Phi}{\partial y} = \nabla^2\Phi \tag{6}$$

where u and v are the x and y velocity components, ξ the vorticity, ψ the stream function, Φ the temperature, Pr $(=\mu C_p/k)$ the Prandtl number and Ra $(=\rho g\beta L^3(T_i - T_o)/\mu\alpha)$ the Rayleigh number. These variables are all dimensionless and the relation with the dimensional quantities is as follows:

$$x = x'/L, \quad y = y'/L, \quad \psi = \psi'/\alpha, \quad \xi = \xi' L^2/\alpha,$$

$$u = u'L/\alpha, \quad v = v'L/\alpha, \quad \Phi = (T - T_o)/T_i - T_o$$

where $L = (D_o - D_i)/2$ is the average gap width and T_i and T_o are the temperatures of the inner and outer tubes.

The boundary conditions on the surfaces of the inner and outer tubes are based on the no-slip, impermeability and isothermal conditions and can be expressed as

$$u = v = \psi = 0, \quad \Phi = 1 \quad \text{for the inner tube}$$

and

$$u = v = \psi = \Phi = 0 \quad \text{for the outer tube.}$$

For $\eta = 0°$ or $180°$ the annulus is symmetrical and only one half of the annulus need be considered. In these cases one more boundary condition is added at the line of symmetry

$$u = \psi = \xi = \frac{\partial v}{\partial x} = \frac{\partial \Phi}{\partial x} = 0.$$

For other values of η the entire field is considered.

A variational finite element method of iterative type was used to solve equations (4)–(6) for $Pr = 0.7$. The finite element mesh was constructed from triangular elements with a total of 396 nodal points (720 elements). Small elements were used in regions where large temperature gradients were expected. A sample of the finite element mesh is shown in Fig. 3.

The numerical procedure was verified by applying it to solve several problems for which analytical, numerical or experimental results are found in the literature. Details of the numerical method and verification are presented in ref. [5].

DISCUSSION OF RESULTS

The mechanism by which vertical eccentricity influences heat transfer at low Rayleigh number can

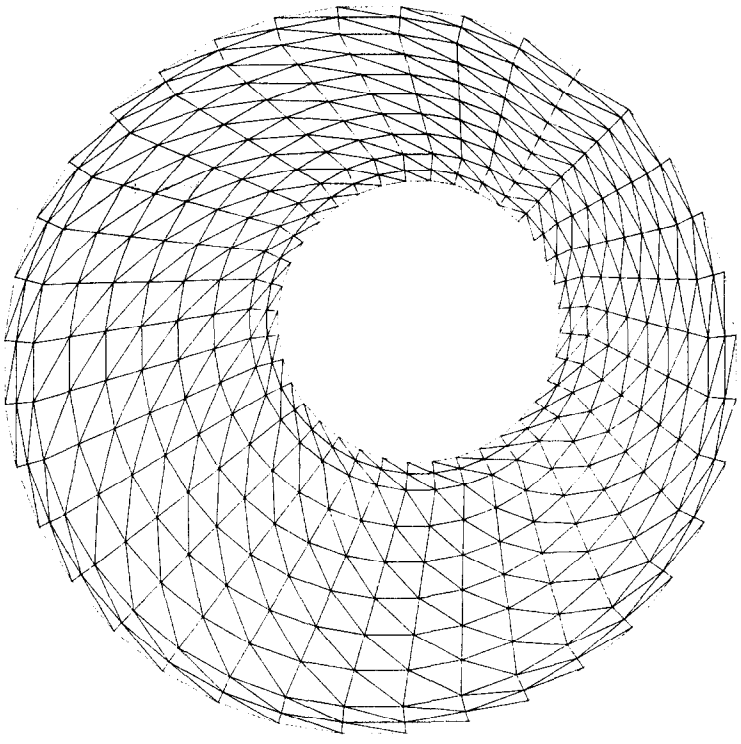

FIG. 3. The finite element mesh used for the case of $e/L = 0.3$, $\eta = 45°$.

be seen in Figs. 4 and 5 which show the temperature profiles and local K_{eq} distributions for two vertical positions of the inner tube, $e/L = 0.6$, $\eta = 0°$, 180° at $Ra = 10^3$. Results for the concentric annulus (Fig. 6) have been included for comparison.

When the inner tube is displaced upward by 60% of the gap width the local K_{eq} distributions change significantly from those of the concentric geometry. On the top of the inner tube, where a minimum existed for the concentric annulus, there is a local maximum due to the reduced resistance to conduction in the narrow gap. However, on the lower portion of the inner tube it is evident that convection is dominant, since the local K_{eq} distribution remains much the same as for the concentric geometry even though the gap is much wider. The outer tube also exhibits high local heat transfer in the narrow gap region due to conduction, but on the lower portion of the outer tube the local K_{eq} value drops to an extremely low value due to the reduced convective flow in this region.

The temperature profile plots and the local K_{eq} distributions for $e/L = 0.6$, $\eta = 180°$ (Fig. 5) indicate enhanced convection. The temperature profile for $\theta_i = 30°$, which passes through the convective cell, shows that the temperature gradient near the core of the cell is low. Heat is being convected around the core rather than being conducted through it. In contrast, the $\theta_i = 30°$ scan for the concentric geometry (Fig. 6) shows a significant temperature gradient in the central region of the gap. These stronger convective velocities for downward displacement have the most

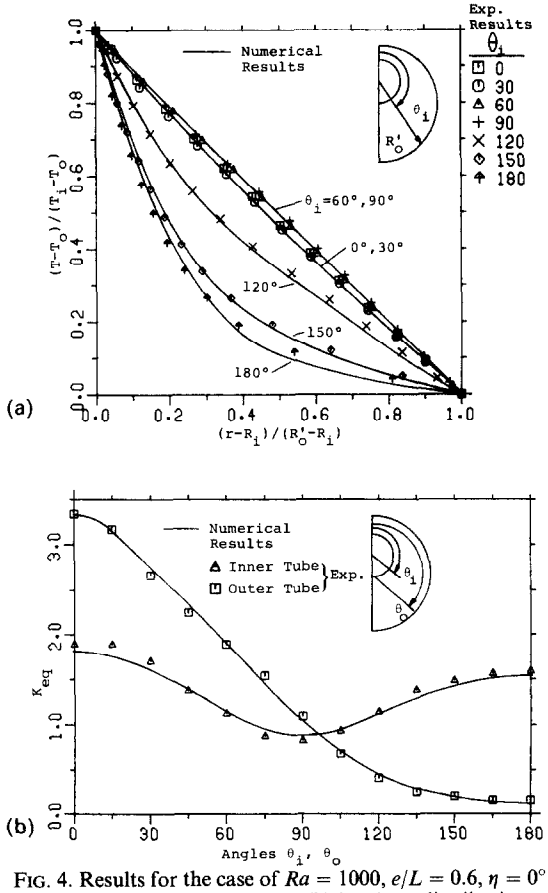

FIG. 4. Results for the case of $Ra = 1000$, $e/L = 0.6$, $\eta = 0°$: (a) temperature distribution; (b) local K_{eq} distribution.

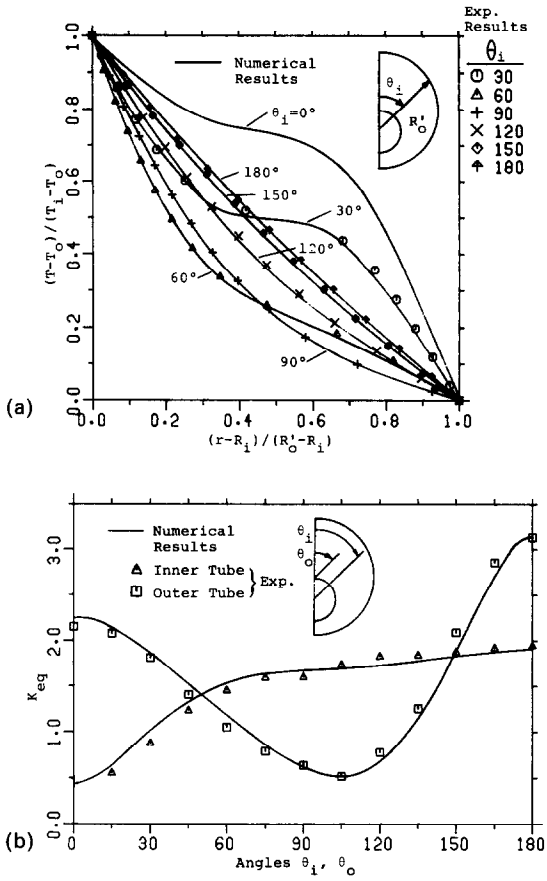

FIG. 5. Results for the case of $Ra = 1000$, $e/L = 0.6$, $\eta = 180°$: (a) temperature distribution; (b) local K_{eq} distributions.

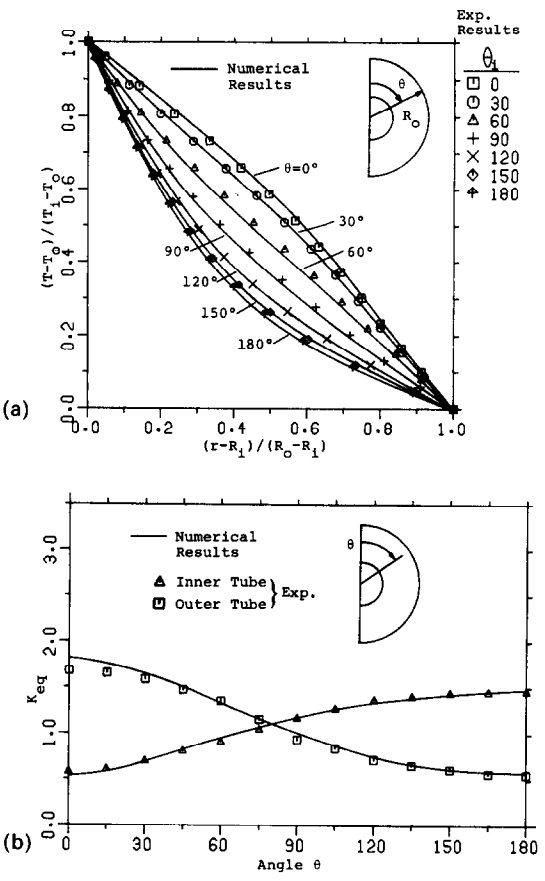

FIG. 6. Results for the case of $Ra = 1000$, $e/L = 0$: (a) temperature distribution; (b) local K_{eq} distributions.

influence on the local heat transfer on the top of the inner and outer tube. The stronger plume rising off the inner tube causes a lower minimum on the top of the inner tube and a greater maximum on the top of the outer tube.

Figure 7 shows the effect of horizontal eccentricity ($\eta = 90°$) at $Ra = 10^3$ on the thermal and velocity fields in the annulus for an eccentricity ratio of $e/L = 0.6$. The interferogram and numerically obtained isotherms are shown in Figs. 7(a) and (b). Good agreement between these figures was not only found in the general shape of the lines but also in the calculated values of the local heat transfer coefficients. One can easily notice that the plume is not rising vertically above the inner tube. Rather, due to a stronger recirculating vortex in the wide gap region, the plume is shifted off the top of the inner tube. The streamlines for this case, given in Fig. 7(c), show that with increasing eccentricity the convective cell in the narrow gap region becomes smaller and weaker and may even break down into two small cells.

Figure 8(a) shows the influence of Rayleigh number on the outer tube's local K_{eq} distribution for horizontal eccentricity of $e/L = 0.6$. The analytical solution for pure conduction is shown for comparison. For pure conduction the maximum heat transfer occurs at $\theta_o = 90°$, the location of the minimum gap width. In this region conduction dominates the local heat transfer even at $Ra = 1.5 \times 10^3$. In the wide gap region, the transition from conduction to convection is evident. For pure conduction the minimum heat transfer occurs at $\theta_o = 270°$. With increasing Rayleigh number the conductive resistance presented by the gap has less effect and the minimum shifts toward the outer tube's lower stagnation point. Also, the strengthening plume rising off the inner tube produces a local maximum at $\theta_o \approx 345°$.

Similar trends are evident in the inner tube K_{eq} distribution for $e/L = 0.6$ ($\eta = 90°$) shown in Fig. 8(b). Where the gap is the narrowest, conduction dominates. Also, the minimum heat transfer location shifts from the widest gap location ($\theta_i = 270°$) for $Ra = 0$ to the plume location $\theta_i = 330°$ for $Ra = 1.5 \times 10^3$ as convection develops. For convection, the local heat transfer on the inner tube rod in the vicinity of the plume ($\theta_i \approx 330°$) is lower than the value for pure conduction and decreases with increasing Rayleigh number. The location where the local heat transfer first drops below the conduction curve ($\theta_i \approx 300°$) occurs higher on the inner tube with

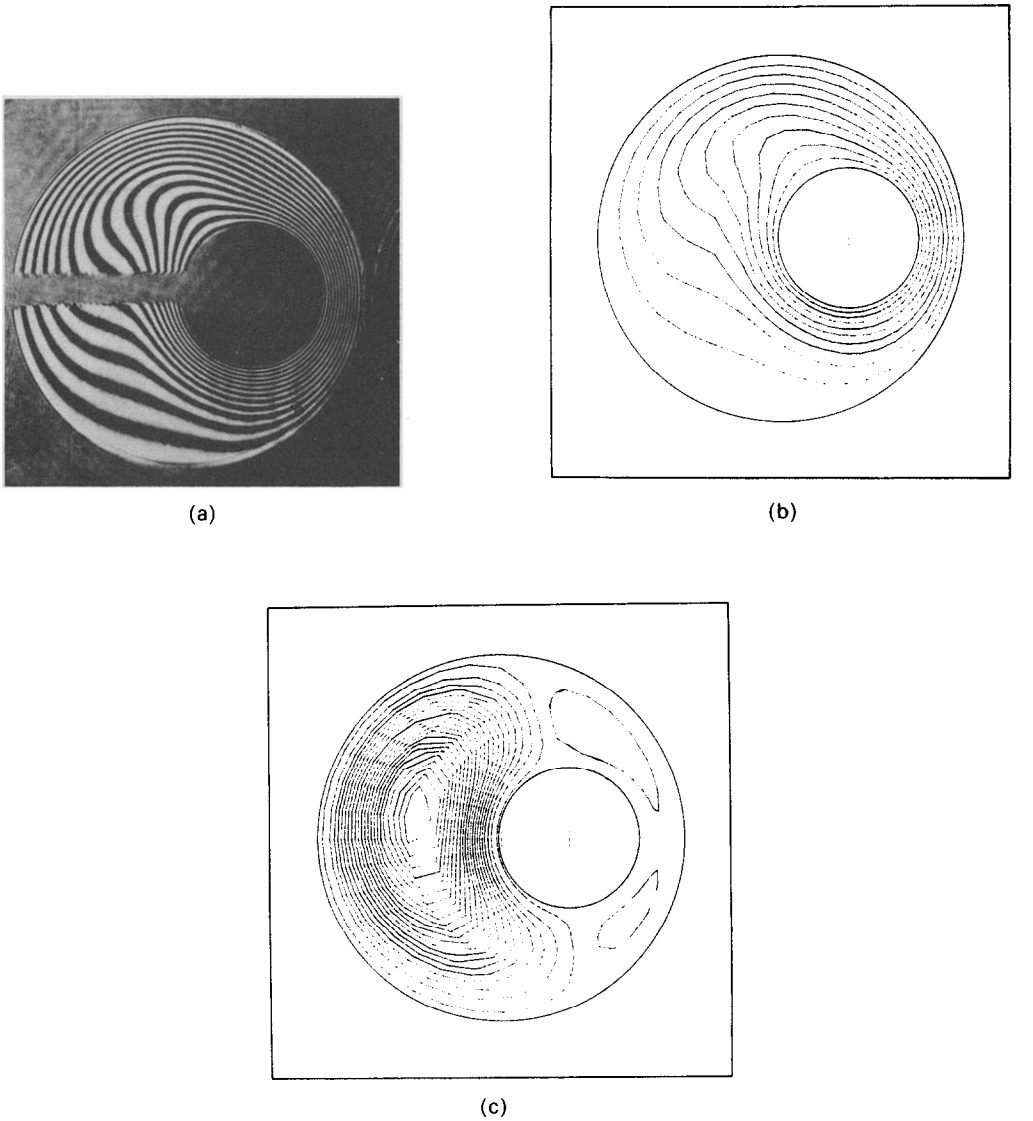

FIG. 7. The experimental and numerical results for the case of $Ra = 1000$, $e/L = 0.6$, $\eta = 90°$: (a) interferogram; (b) isotherms; (c) streamlines.

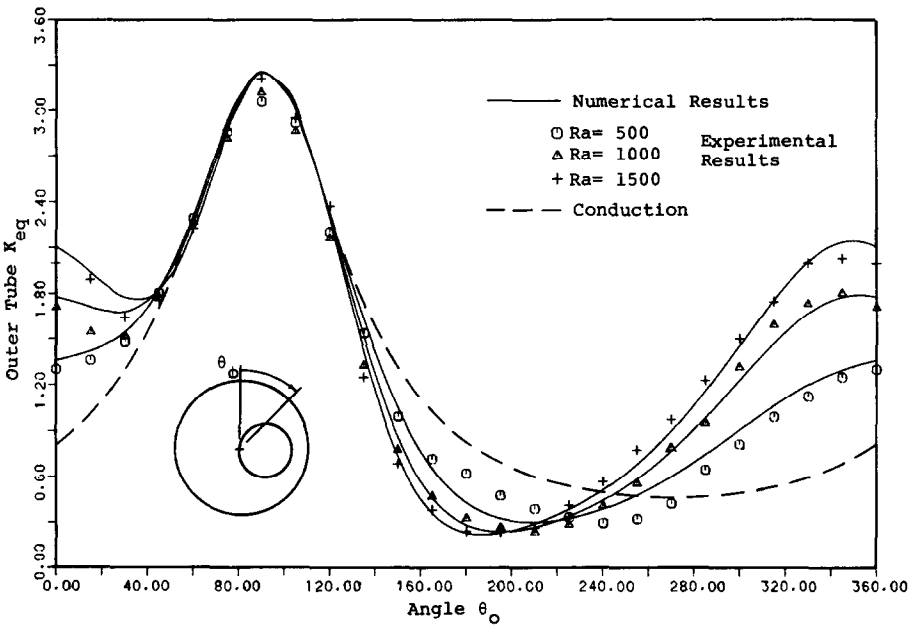

(a)

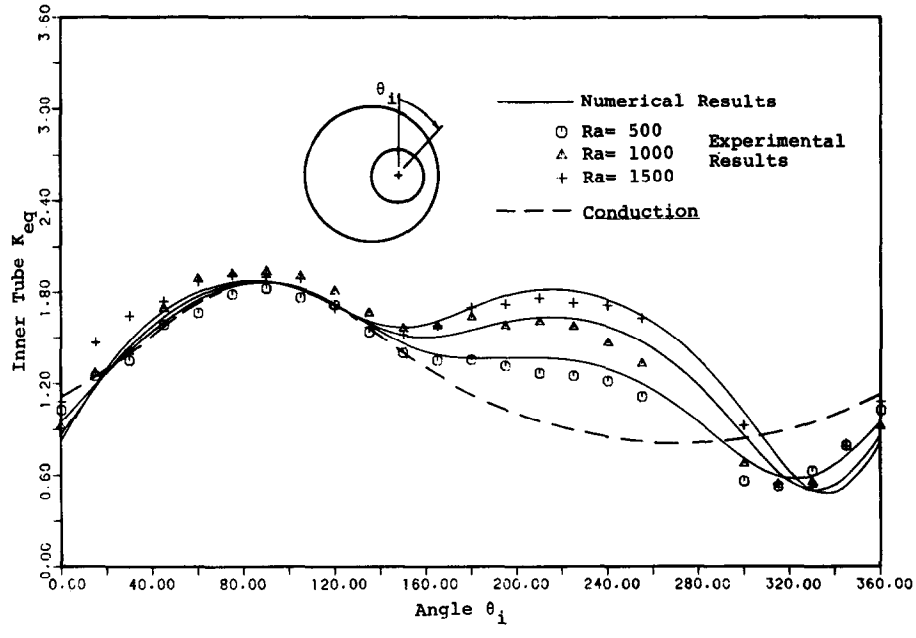

(b)

FIG. 8. The local K_{eq} distributions for the case of $e/L = 0.6$, $\eta = 90°$: (a) outer tube; (b) inner tube.

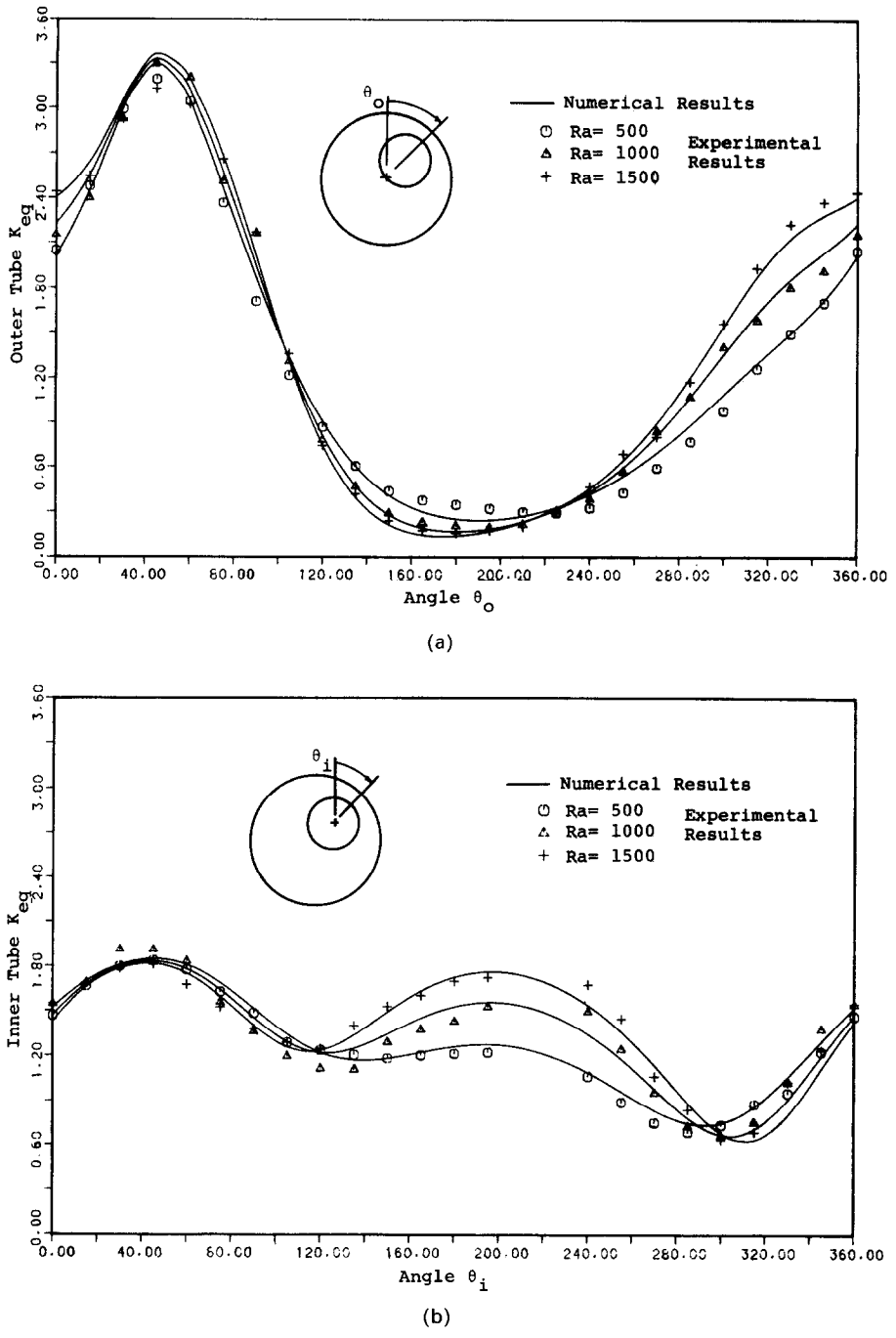

FIG. 9. The local K_{eq} distributions for the case of $e/L = 0.6$, $\eta = 45°$: (a) outer tube; (b) inner tube.

increasing Rayleigh number. This shift is expected since at higher Rayleigh number the convective cell strengthens and penetrates higher into the annulus.

The effect of the azimuthal angle on the local K_{eq} distribution is shown in Figs. 9 and 10 for $Ra = 1.5 \times 10^3$ and $e/L = 0.6$. In Fig. 9 where $\eta = 45°$, the maximum value of K_{eq} on the outer tube surface occurs at $\theta_o = 45°$ where the gap width is minimum (conduction) while the minimum value of K_{eq} occurs at the bottom surface near $\theta_o = 180°$ where K_{eq} is very small over a wide area. As η increases to 135° (Fig. 10) the local K_{eq} distribution on the outer tube is found to possess two maximum values instead of one for $\eta = 45°$. The first maximum occurs because of the high conduction heat transfer in the narrow gap ($\theta_o = 135°$) and the second one occurs because of the high temperature gradients due to the rising plume near the top of the outer tube surface.

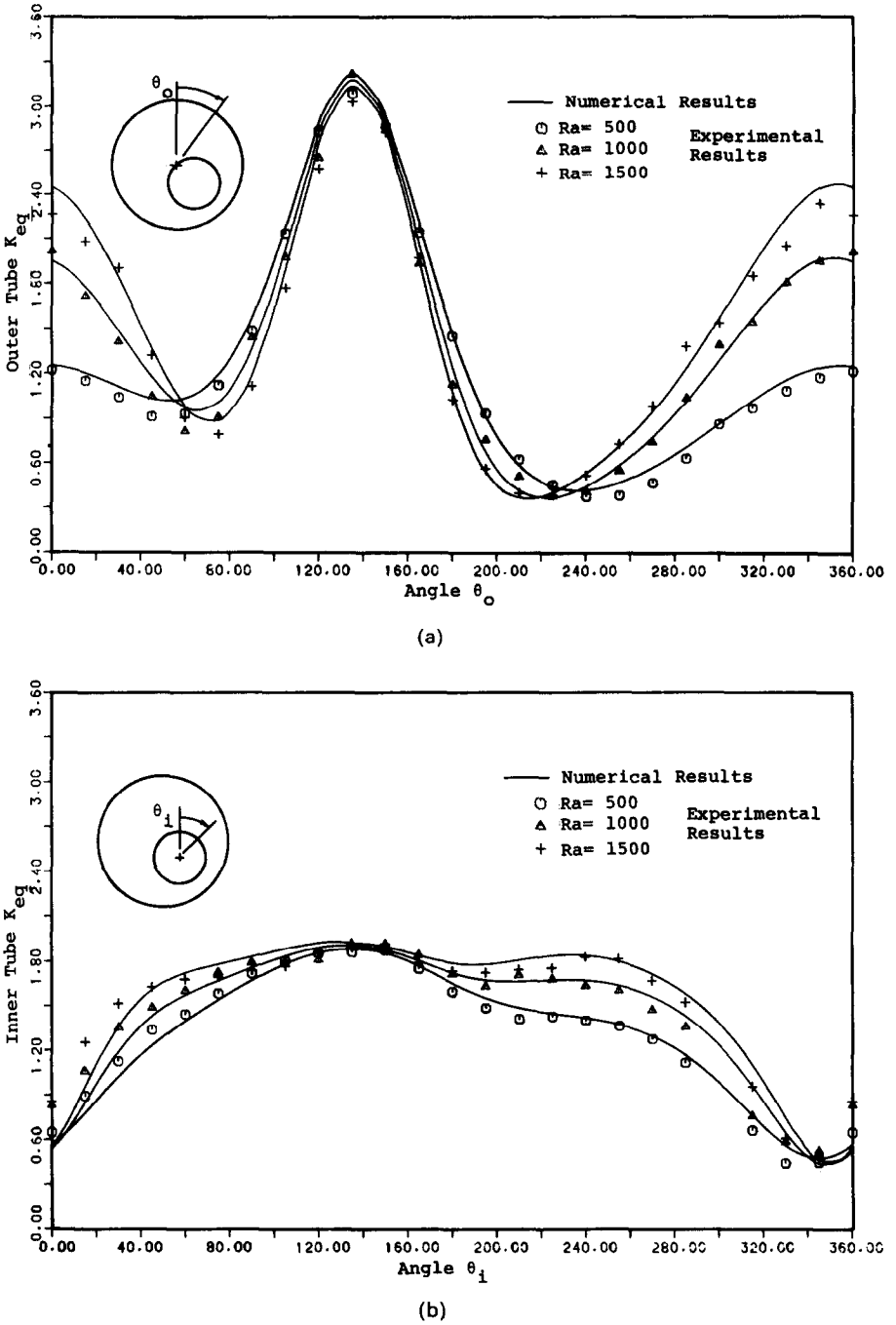

FIG. 10. The local K_{eq} distributions for the case of $e/L = 0.6$, $\eta = 135°$: (a) outer tube; (b) inner tube.

Table 1 shows a comparison between the experimental and the numerical values of $\bar{K}_{eq}$ for various cases. At low Rayleigh number, azimuthal angle has little effect on $\bar{K}_{eq}$, since the heat transfer is almost entirely by conduction. With increasing Rayleigh number, the direction of eccentricity becomes important. The value of $\bar{K}_{eq}$ increases to a maximum at $\eta = 180°$ due to the development of larger and stronger convective cells. With the rod displaced downward $e/L = 0.6$, the experimentally measured $\bar{K}_{eq}$ was 38% greater than for the concentric geometry at $Ra = 10^3$ and 35% greater at $Ra = 1.5 \times 10^3$.

CONCLUDING REMARKS

At low Rayleigh number convection and conduction have a combined influence on heat transfer. The low convective velocities for $Ra < 5 \times 10^2$ redis-

Table 1. A comparison between the experimental and numerical values of $\bar{K}_{eq}$ for various cases

Ra	e/L	η (deg.)	$\bar{K}_{eq}$ exp.	$\bar{K}_{eq}$ numer.	Percentage difference (%)
500	0.3	0	1.050	1.070	1.9
	0.3	45	1.062	1.070	0.7
	0.3	90	1.080	1.077	−0.3
	0.3	135	1.076	1.081	0.5
	0.3	180	1.080	1.088	0.7
	0.6	0	1.269	1.269	0
	0.6	45	1.254	1.272	1.4
	0.6	90	1.261	1.291	2.3
	0.6	135	1.262	1.306	3.3
	0.6	180	1.251	1.334	6.6
1000	0.3	0	1.118	1.121	0.3
	0.3	45	1.106	1.117	1.0
	0.3	90	1.142	1.140	−0.2
	0.3	135	1.171	1.169	−0.2
	0.3	180	1.190	1.208	1.5
	0.6	0	1.339	1.325	−1.0
	0.6	45	1.335	1.334	−0.1
	0.6	90	1.358	1.380	1.6
	0.6	135	1.421	1.435	1.0
	0.6	180	1.488	1.492	0.3
1500	0.3	0	1.193	—	—
	0.3	45	1.173	1.179	0.5
	0.3	90	1.236	1.231	−0.4
	0.3	135	1.271	1.274	0.2
	0.3	180	1.306	—	—
	0.6	0	1.356	—	—
	0.6	45	1.412	1.404	−0.6
	0.6	90	1.464	1.469	0.3
	0.6	135	1.514	1.539	1.6
	0.6	180	1.567	—	—

tribute the local heat transfer but do not appreciably change $\bar{K}_{eq}$. For $Ra = 5 \times 10^2$, $\bar{K}_{eq}$ depends primarily on the magnitude of eccentricity and has very little dependency on eccentricity angle.

For $Ra > 5 \times 10^2$ eccentricity angle becomes increasingly important. The maximum overall heat transfer occurs at $\eta = 180°$ since this geometry is most conducive to the formation of strong convective cells in the wide gap region above the inner tube. In the transition regime, the effect of eccentricity on $\bar{K}_{eq}$ is greater than observed by Kuehn and Goldstein [4] in the boundary layer regime. The experimental and numerical results showed a good agreement.

Acknowledgements—The authors wish to acknowledge the support received from the NSERC of Canada and the King Fahd University of Petroleum & Minerals during the course of this study.

REFERENCES

1. Y. A. Koshmarov and A. Y. Ivanov, Experimental study of heat transfer through a rarefied gas between coaxial cylinders, *Heat Transfer—Sov. Res.* **5**(1), 29–36 (1973).
2. S. D. Probert, D. Sadhu and D. Syed, Thermal insulation provided by annular air-filled cavities, *Appl. Energy* **1**, 145–153 (1975).
3. E. van de Sande and B. J. G. Hamer, Steady and transient natural convection in enclosures between horizontal circular cylinders (constant heat flux), *Int. J. Heat Mass Transfer* **22**, 361–370 (1979).
4. T. H. Kuehn and R. J. Goldstein, An experimental study of natural convection heat transfer in concentric and eccentric horizontal cylindrical annuli, *ASME J. Heat Transfer* **100**, 635–640 (1978).
5. H. M. Badr, Study of laminar free convection between two eccentric horizontal tubes, *Trans. CSME* **7**(4), 190–196 (1983).
6. J. Prusa and L. S. Yao, Natural convection heat transfer between eccentric horizontal cylinders, *ASME J. Heat Transfer* **105**, 108–116 (1983).
7. C. H. Cho, K. S. Chang and K. H. Park, Numerical simulation of natural convection in concentric and eccentric horizontal cylindrical annuli, *ASME J. Heat Transfer* **104**, 624–630 (1982).
8. U. Projahn, H. Rieger and H. Beer, Numerical analysis of laminar natural convection between concentric and eccentric cylinders, *Numer. Heat Transfer* **4**, 131–146 (1981).
9. D. Naylor, An interferometric study of natural convection in horizontal eccentric annuli, M.E.Sc. thesis, University of Western Ontario, London, Ontario (1985).

ETUDE EXPERIMENTALE ET NUMERIQUE DE LA CONVECTION NATURELLE ENTRE DEUX TUBES EXCENTRES

Résumé—Une étude expérimentale et numérique est conduite sur le transfert thermique par convection naturelle autour d'un tube entouré par un autre tube isotherme. Des résultats expérimentaux sont obtenus par interférométrie Mach–Zehnder et les équations du problème sont traitées numériquement en utilisant une méthode variationnelle d'éléments finis. On s'intéresse particulièrement à l'effet de l'excentricité du tube interne et de l'angle azimuthal sur le champ thermique dans l'espace annulaire. Des résultats sont obtenus pour l'air à trois nombres spécifiques de Rayleigh dans le régime de transition, $Ra = 5 \times 10^2$, 10^3 et $1{,}5 \times 10^3$.

EXPERIMENTELLE UND NUMERISCHE UNTERSUCHUNG DER NATÜRLICHEN KONVEKTION ZWISCHEN ZWEI EXZENTRISCHEN ROHREN

Zusammenfassung—Der Wärmeübergang bei natürlicher Konvektion von einem isothermen Innenrohr an ein umgebendes isothermes Außenrohr wird sowohl experimentell als auch numerisch untersucht. Die experimentellen Ergebnisse erhält man unter Verwendung eines Mach-Zehnder-Interferometers. Die Grundgleichungen werden mit Hilfe einer veränderlichen Finite-Elemente-Methode gelöst. Der Schwerpunkt wird dabei auf den Einfluß der Exzentrizität des Innenrohres und der Lage des Azimutwinkels auf das Temperaturfeld im Ringraum gelegt. Für Luft wurden bei drei bestimmten Rayleigh-Zahlen, $Ra = 5 \times 10^2$, 10^3, $1{,}5 \times 10^3$, im Übergangsbereich Ergebnisse ermittelt.

ЭКСПЕРИМЕНТАЛЬНОЕ И ЧИСЛЕННОЕ ИССЛЕДОВАНИЕ ЕСТЕСТВЕННОЙ КОНВЕКЦИИ В ЗАЗОРЕ МЕЖДУ ДВУМЯ НЕКОАКСИАЛЬНЫМИ ТРУБАМИ

Аннотация—Проведено экспериментальное и численное исследование теплопереноса естественной конвекцией в кольцевом зазоре от горизонтальной изотермической внутренней трубы к изотермической наружной. Экспериментальные данные получены при помощи интерферометра Маха–Цендера. Определяющие уравнения решались численно вариационным методом конечных элементов. Особое внимание обращено на влияние эксцентриситета и азимутального углового положения внутренней трубы на тепловое поле в кольцевом зазоре. Получены результаты для воздуха при трех характерных значениях числа Рэлея в переходном режиме: $Ra = 5 \times 10^2$, 10^3, $1{,}5 \times 10^3$.